Environmental Science Advances

ROYAL SOCIETY OF CHEMISTRY

PAPER

View Article Online
View Journal | View Issue



Cite this: *Environ. Sci.: Adv.*, 2022, **1**, 156

# Single-entity coccolithophore electrochemistry shows size is no guide to the degree of calcification†

Minjun Yang,[a] Christopher Batchelor-McAuley,[a] Samuel Barton,[b] Rosalind E. M. Rickaby,[b] Heather A. Bouman[b] and Richard G. Compton *[a]

Received 7th February 2022
Accepted 25th March 2022

DOI: 10.1039/d2va00025c

rsc.li/esadvances

We report single-entity measurements of the degree of calcification of individual phytoplankton cells. Electrogenerated acid is used to dissolve the calcium carbonate ($CaCO_3$) shell (coccosphere) of individual coccolithophores and the changes in size are monitored by simultaneous optical measurements, allowing the $CaCO_3$ content of the single phytoplankton cell to be inferred *via* analysis of the dissolution kinetics. Three species of coccolithophore, *E. huxleyi*, *G. oceanica* and *C. braarudii*, were studied with $CaCO_3$ masses measured over 3 orders of magnitude ranging from 2.6 pg to 8.3 ng of $CaCO_3$ per cell. Surprisingly, within a species, the $CaCO_3$ content is not correlated to the size of the coccosphere but the volume of its shell. Further, the variation of the $CaCO_3$ content with the cell size and the particulate inorganic carbon (PIC) to particulate organic carbon (POC) ratio at different stages of the growth phase is reported.

### Environmental significance

Marine calcifiers, coccolithophores, are responsible for sequestering more than $10^{15}$ g of atmospheric $CO_2$ per year to the deep ocean as $CaCO_3$. This is directly comparable to the rate of released by humans. Coccolithophores play a crucial part in the marine carbon cycle and are jeopardised by climate change. There is currently no way of measuring the mass of biogenic calcite of individual coccolithophores. This work presents a proof-of-concept approach combining optics with electro-generated acid to "titrate" the biogenic calcite of each of the coccolithophores. The amount of acid reacted reveals the mass of biogenic calcite (pico- to nano-grams) and we show that, surprisingly, size is no good indication of the calcification degree.

## Introduction

Single-entity measurement is often the ultimate challenge in any scientific discipline. At the most basic level, characterising the behaviour of a single unit in any system, for example, in catalysis, cellular biology, enzyme or reaction kinetics, allows the ensemble response to be better understood and optimised. In the modern era, with advances in electronic components and with a large arsenal of redox systems at the user's disposal, electrochemistry has claimed notable successes in stochastic measurements[1] in the detection of, but not limited to, single nanoparticles,[2] electrocatalysis,[3,4] red blood cells,[5] bacteria[6,7] and viruses.[8]

In the world's ocean, calcifying marine phytoplankton – coccolithophores – play a crucial role in the global carbon cycle[9] owing to their ability to sequester in excess of $10^{15}$ g of $CaCO_3$ to the deep ocean per annum.[10,11] For the past tens of millions of years, coccolithophores, alongside foraminifera, have been the dominant pelagic calcifiers.[10] These microscopic unicellular species bioaccumulate elaborate plates of $CaCO_3$ (coccoliths) in open-surface waters ultimately encrusting themselves with inter-locking coccoliths (coccospheres, Fig. 1).[12] The dense $CaCO_3$ shell (particulate inorganic carbon, PIC) act as 'ballast' and provides protection towards bio-remineralization of particulate organic carbon (POC) as it traverses down the water column forming a continuous flux of carbon to the deep, where it is stored for millennia.[13,14]

This ability of the ocean to sequester atmospheric $CO_2$ to the deep is generally referred to as the biological carbon pump.[15,16] This occurs at a global scale and the rate of $CO_2$ export to the deep ocean is directly comparable to that released by mankind.[17] However, the ability of coccolithophores to continue to biomineralize $CaCO_3$ (PIC) under conditions of "climate crisis" is unclear due to different species- and strain-specific responses towards changes such as pH, illumination and sea surface temperature conditions.[18] The mass of particulate inorganic and organic carbon sequestered by coccolithophores, PIC and POC respectively, and also the 'rain-ratio' of PIC : POC, provides

[a]*Physical and Theoretical Chemistry Laboratory, Department of Chemistry, University of Oxford, South Parks Road, Oxford, UK. E-mail: Richard.Compton@chem.ox.ac.uk*
[b]*Department of Earth Sciences, University of Oxford, South Parks Road, Oxford, UK*

† Electronic supplementary information (ESI) available. See DOI: 10.1039/d2va00025c

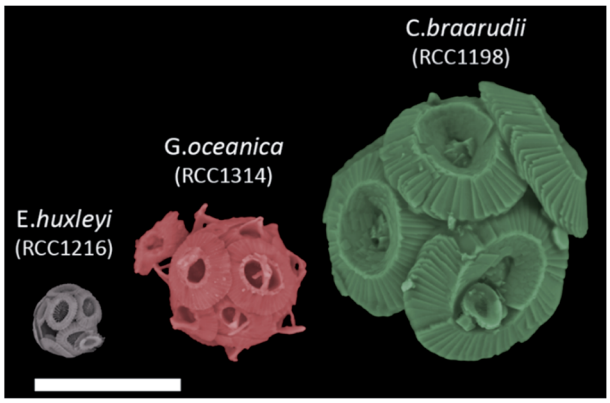


Fig. 1 False coloured SEM images of *E. huxleyi*, *G. oceanica* and *C. braarudii* coccosphere at day 9 of incubation. Scale bar = 10 μm.

crucial information to feed into global models of the carbon cycle for accurate assessment of the impacts of anthropogenic change.[19,20]

Coccoliths are the predominant form of $CaCO_3$ on the ocean floor with ancient fossils dating as far back as 225 million years.[21] Single coccoliths may become detached from coccolithophores either during the lifecycle of the latter or after cellular death. Although existing techniques allow the PIC content of individual coccoliths to be either measured[22–24] or estimated,[25] this, ultimately, provides calcification information about the past, not the present. To monitor and predict the imminent threat of climate change on our dominant open-ocean calcifiers we must quantify the PIC content bioaccumulated by coccolithophores in the present marine environment. Currently, there are two methods to quantify PIC contents per coccolithophore. First, an ensemble of coccolithophores is filtered and treated, or not, with acid, with the difference in the carbon mass between the two samples measured *via*, for example, elemental analysis providing the total $CaCO_3$ content of the ensemble prior to acid dissolution.[26,27] By dividing the total PIC content of the ensemble by the estimated number of coccolithophore cells present, a PIC cell$^{-1}$ value can be estimated. Second, alternatively, by obtaining the average coccolith mass from either direct measurements or an estimation of the average coccolith length and shape factor,[25] the PIC content of a coccolithophore can be approximated by multiplying by the estimated number of coccoliths.[28,29] Note that the size of the coccoliths on any coccolithophore can vary by up to ~50%[30] and the number of coccolith per cell can only be estimated if the number of coccoliths can be seen, which is not possible *via* traditional scanning electron microscopy (SEM),[26] which inevitably precludes the 3-dimensional imaging needed. However, more sophisticated 3D techniques such as X-ray nanotomography[30] and focused ion beam combined with SEM[31] allows individual coccolithophores to be reconstructed in 3D, thus providing a measure of individual coccolithophore PIC contents, but such approaches are extremely expensive and time consuming.

More recently, proof-of-concept electrochemical methods have shown their ability to identify, in combination with fluorescence spectroscopy, the speciation of marine phytoplankton and,[32] separately, single-entity measurement of detached coccolith $CaCO_3$ masses.[22] In the present study, electrochemistry is utilised to provide a high-throughput single-entity PIC content measurement of *living* coccolithophores. Herein, acid is generated electrochemically to dissolve away the $CaCO_3$ shell of the individual coccolithophores to reveal the underlying 'naked' cell. *In situ* optical imaging reveals the dissolution kinetics which is used to accurately infer the PIC content of coccolithophores on a single-entity basis. Then the size of the 'naked' cell after complete acid dissolution, as measured by optics, provides an estimation of POC content which, in combination with the former measurement, allows the ratio of PIC : POC to be inferred.

## Experimental section

See ESI.†

## Results and discussion

The following work utilises electrochemistry to induce acid dissolution of three coccolithophores species revealing their biomineralized calcium carbon contents ($CaCO_3$, PIC) on a single-entity basis. The three species under investigation are *Emiliania huxleyi*, *Gephyrocapsa oceanica* and *Coccolithus pelagicus* subsp. *braarudii*. By dissolving away the $CaCO_3$ *via* electrogenerated acid with optical imaging, a range of cellular properties are extracted on a single-entity basis: plankton size before *and* after complete acid dissolution revealing the shell thickness and size of the underlying biological cell, PIC content of the calcareous shell and an estimation of the PIC : POC ratio. Moreover, these experiments are conducted at different parts of the growth curve to reveal the variation of the above-mentioned properties due to the change in physiology.

Fig. 1 shows representative SEM images of the three species of coccolithophores at day 9 of growth. The largest of the three species, *C. braarudii*, measures ~20 μm in diameter whereas *E. huxleyi* is approximately 4 times smaller with a diameter of around 5 μm. Moreover, from the SEM images, one can see that on an individual coccolith level, not only the size differs from one species to another, but there is also a change in both the morphology and 'solidity' of the coccoliths produced. Fig. S1† shows the surface elemental mapping of the three coccolithophores using energy-dispersive X-ray microscopy (EDX). A relatively high ratio atom percentage of carbon (~35%) and oxygen (~53%) was measured to that of calcium (~10%) for pure $CaCO_3$. Note that this ratio is not reflective of the entire coccosphere as EDX rays penetrate only microns below the surfaces. The high ratio of measured carbon and oxygen signal, compared to that expected from $CaCO_3$, likely reflects the polysaccharide present on the surface of coccoliths, which accounts for less than 3% of the coccolith by mass.[33]

To estimate the total PIC content of the coccospheres, at the crudest level one might initially simply assume the coccosphere is a solid 'ball' of calcite and upscale the measured radius ($r$)

obtained *via* SEM or other imaging techniques, by the density of calcite ($\rho_{CaCO_3} = 2.71$ g cm$^{-3}$ (ref. 34))

$$\mathrm{PIC} = \frac{4}{3}\pi r^3 \rho_{CaCO_3} \quad (1)$$

This, however, over-estimates the $CaCO_3$ mass because first, the underlying biological cell is particulate organic carbon (POC) and should be separated from PIC calculation, second, due to the nature of interlocking coccoliths the unfilled voids are not accounted for, and third, coccoliths are not perfect discs and therefore the volume of each disc is smaller than a short-cylinder of the same geometric size. To overcome these challenges, we dissolve away the calcareous shell by generating acid controllably *via* electrochemistry whilst imaging the changes in the coccolithophore *via in situ* optical imaging.

Fig. 2a illustrates the physicochemical processes that occur in such opto-electrochemical experiments. A coccolithophore residing on the electrode is exposed to electrogenerated acid which reacts with the calcareous shell of the coccolithophore leading to the full dissolution of the latter revealing the underlying 'naked' cell. Under strong acid conditions, acid dissolution of calcite goes to completion and consumes two stoichiometric equivalents of protons[35]

$$CaCO_3(s) + 2H^+(aq) \rightarrow Ca^{2+}(aq) + CO_2(g) + H_2O(l) \quad (2)$$

Fig. 2b shows the 3D-printed cell in which the opto-electrochemical experiments were conducted. The 3D-printed cell facilitates a three-electrode setup with a reaction chamber approximately 1 cm$^3$ in volume and is fully discussed in the Experimental section in the ESI.† Synchronised optical images of the coccolithophores are taken following the switch-on of the electrochemical proton formation revealing the dissolution of *each* coccosphere present on the electrode surface to allow single-entity measurements to be made. Kinetic information is inferred by monitoring the shrinkage of the $CaCO_3$ shell and allows the total PIC content of the coccosphere to be calculated, as discussed below, and the size of the 'naked' coccolithophore cell provides an estimate for the particulate organic carbon (POC) content, as will also be discussed below.

Prior to the electrochemical dissolution, coccolithophore samples were dropcasted onto a glassy carbon electrode (diameter = 3 mm). The surface of the electrode acts as a supporting substrate for the coccolithophores and as a mean for electrochemically generating acid. The solution chamber was then filled with 0.7 M KCl inert electrolyte with 20 mM $Ca^{2+}$ and millimolar concentrations of hydroquinone (2 mM for *G. oceanica* and *E. huxleyi*, and 10 mM for *C. braarudii*). 20 mM of $Ca^{2+}$ was used to prevent the dissolution of biogenic calcite prior to the start of the experiment, discussed in detail in ESI Section 3,† and hydroquinone was used as an acid precursor which releases two stoichiometric equivalents of protons when electrochemically oxidised at the electrode interface (Scheme 1).[22]

Shown in Fig. 2c are optical images of a representative *C. braarudii* coccosphere undergoing electrochemically induced acid dissolution with 10 mM of hydroquinone. The top row of images shown in Fig. 2c are raw images obtained directly from

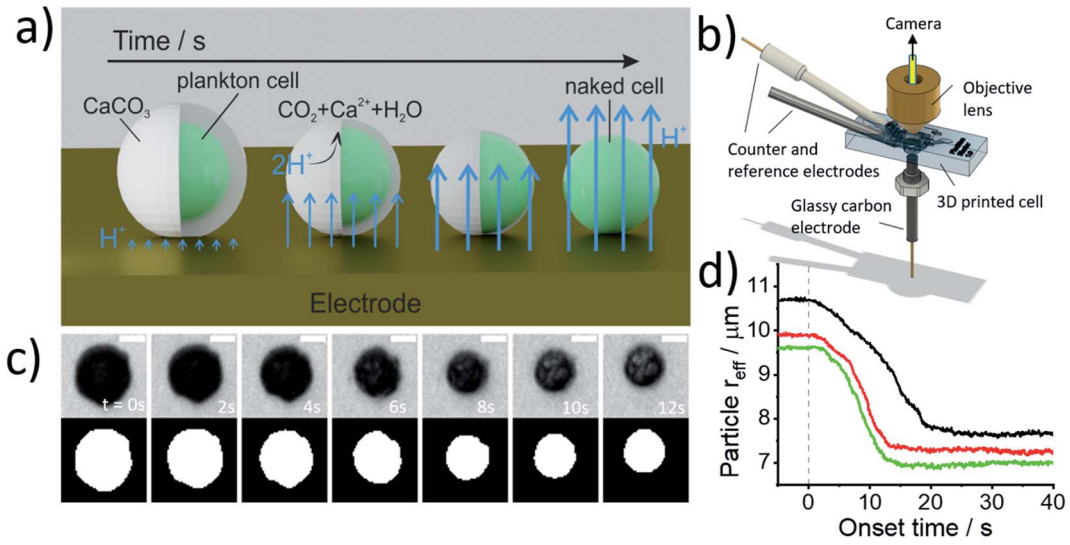


Fig. 2 (a) A schematic image depicting the electrogenerated acid dissolution of a coccosphere. Initially, a coccolithophore cell is stationary on the surface of an electrode. At the start of the experiment a *ca.* millimolar level concentration of electrogenerated acid is formed at the electrode interface to dissolve off the $CaCO_3$ shell revealing the underlying biological cell which is inert to acid dissolution. (b) Schematic diagram of the 3D-printed opto-electrochemical cell. Coccolithophores were dropcasted onto the glassy carbon electrode prior to the opto-electrochemical experiment. (c) Optical images of an individual *C. braarudii* undergoing acid dissolution. At $t = 0$, a potential of +1.0 V *vs.* SCE is applied to the glassy carbon electrode bathed in an aqueous solution containing 10 mM of hydroquinone $H_2BQ$(aq), 20 mM $CaCl_2$ and 0.7 M KCl. The top row shows the optical images as recorded by the camera from a top-down view. The bottom row of images is those after image thresholding which are used to calculate the effective particle radius ($r_{eff} = (\mathrm{area}/\pi)^{0.5}$). Scale bar = 10 µm. (d) A plot of the effective particle radius as a function of potential onset time for three representative *C. braarudii* individuals. Each line represents a single *C. braarudii* cell.

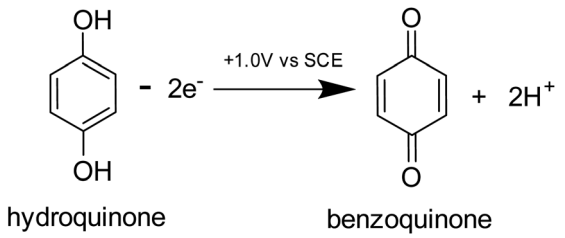


Scheme 1 The oxidation reaction of hydroquinone to benzoquinone.

the camera and the bottom row are those after image thresholding which is used to calculate the effective radius of the coccosphere during the experiment, assuming a perfect circle (area $= \pi r_{\mathrm{eff}}^2$, where $r_{\mathrm{eff}}$ is the radius of a circle of equivalent area to the image of the coccolithophore). An anodic potential of +1.0 V *vs.* saturated calomel electrode (SCE) was applied to the working electrode to initiate the release of a local concentration of approximately millimolar of $H^+$. As can be seen in Fig. 2c, within tens of seconds of the acid generation, the calcium carbonate shell of the coccolithophore is seen to dissolve completely to reveal the underlying 'naked' biological cell. The cell-wall composition of the 'naked' cell is typically cellulose or similar polysaccharide based.[36] The change in the effective coccolithophore radius, $r_{\mathrm{eff}}(t)$, is plotted in Fig. 2d for three representative *C. braarudii* coccospheres studied after 9 days of growth (see ESI Section 1† for cell cultures). The effective coccosphere radius, $r_{\mathrm{eff}}$, is seen to decrease quasi-linearly as a function of time after the generation of acid until it reaches a constant value of around 7–8 μm. It is clear that the decrease in coccolithophore size is associated with the acid-dissolution of biogenic calcite (eqn (2)) and the underlying biological cell is 'inert' to acid attack over the timescale of this experiment. Before the calcite dissolution kinetics are discussed, first, on the most basic level, the $r_{\mathrm{eff}}(t)$ transients provide direct physiological properties of the coccolithophore, size with and without the shell.

Fig. 3 plots the size of the individual coccolithophores measured optically, before and after, complete acid dissolution. Each data point represents data for an individual coccolithophore and the colour represents the 'age' of the culture sample from day 1 (blue) to day 17 (yellow) since the initial inoculation. Note that data below the dashed reference line is an indication of some form of a calcareous shell, which is dissolved under acid attack. The size of the coccolithophores, before and after complete acid dissolution, is in agreement with that seen under SEM and decreases in the order of: *C. braarudii* > *G. oceanica* > *E. huxleyi*. Due to the limitation of the wavelength of light used in optical measurements, the sizing measured herein is found to overestimate by approximately 0.5 μm as compared to those measured in SEM. This is fully discussed as part of the measurement uncertainties in ESI Section 5.† As can be seen in Fig. 3, the distribution of coccosphere and cellular size of *C. braarudii* and *E. huxleyi* are relatively invariant over 17 days of growth. On the other hand, towards the later stage of the growth phase, a thinner calcareous shell is seen on *G. oceanica* coccospheres. Separately, when the experiments were conducted in $Ca^{2+}$-free electrolytes, the predominant data points for *E. huxleyi* and *G. oceanica* in their early growth phase overlay on the $y = x$ reference line (Fig. S3†). This is because the time required to set up the opto-electrochemical experiment after filling the reaction chamber with $Ca^{2+}$-free electrolyte, which is approximately 1–2 minutes, is sufficient to dissolve away the biomineralized $CaCO_3$ prior to the onset of electro-generation of acid at $t = 0$. In the later growth phase, however, *E. huxleyi* and *G. oceanica* were not completely 'deshelled' in $Ca^{2+}$-free electrolyte at the onset of the electro-generated acid. This is likely because of a higher number density of coccospheres, and detached coccoliths, present on the surface of the electrode resulting in an overlap of the diffusion field[37,38] causing a local saturation of $Ca^{2+}$ and $HCO_3^-$. Complete 'deshelling' of the *C. braarudii* coccospheres was not seen by the exposure of 1–2 minutes in $Ca^{2+}$-free electrolyte. This likely reflects a much larger quantity of calcite is present on *C. braarudii* as revealed below. Having discussed the physicochemical processes that occur in the opto-electrochemical experiment, we next examine and discuss the different growth phases of the coccolithophores over 17 days following the initial inoculation.

Fig. 4a–c plots the measured cellular density of the coccolithophores in the growth medium over a 17 day period following inoculation. For all three species, a 'lag' phase in growth is seen in days 0–1 as time is typically required for them to acclimate to

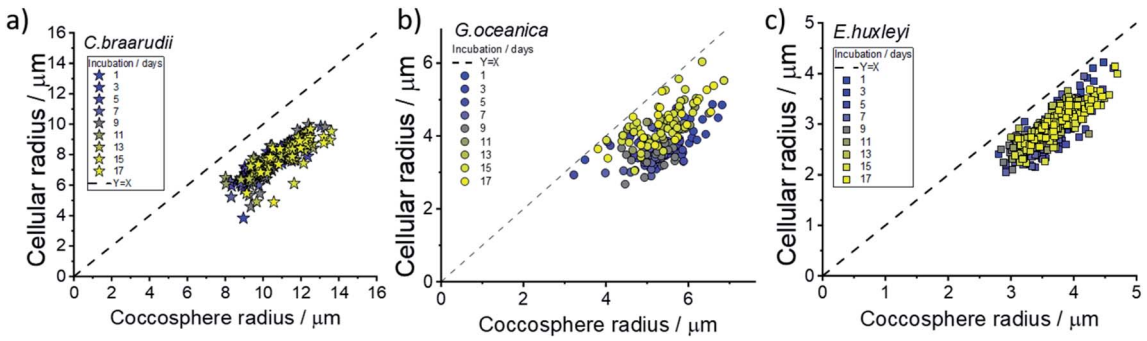


Fig. 3 The effective radius of coccolithophores after complete acid dissolution plotted against that prior to acid dissolution. Speciation of coccolithophores: (a) *C. braarudii*, (b) *G. oceanica* and (c) *E. huxleyi*. The dotted line represents the $y = x$ line corresponding to no $CaCO_3$ shell. The electrolyte contains 10 mM of hydroquinone $H_2BQ$(aq), 20 mM $CaCl_2$ and 0.7 M KCl.

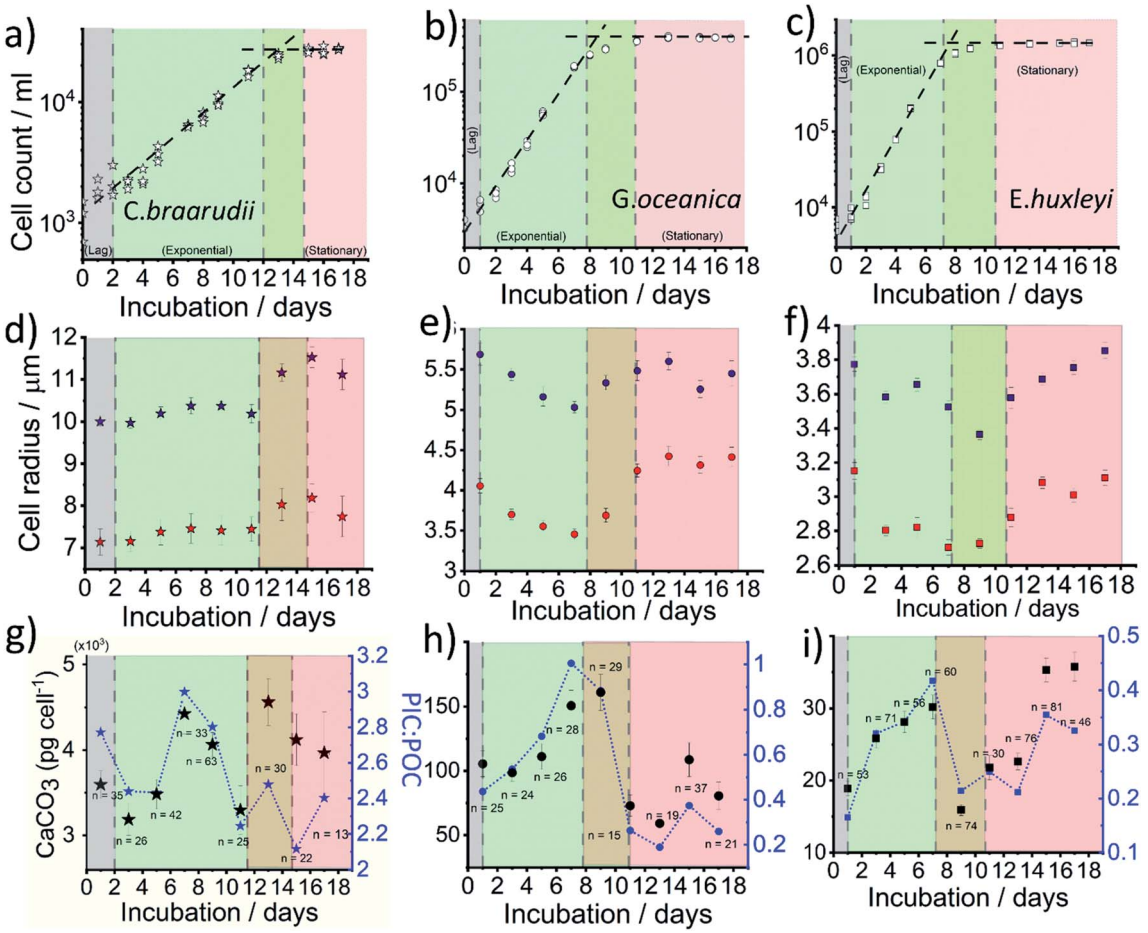


Fig. 4 Physical parameters of coccolithophores obtained as a function of growth for *C. braarudii* (a, d and g), *G. oceanica* (b, e and h) and *E. huxleyi* (c, f and i). All experiments were conducted between 2–4 pm on the day of measurement. (a–c) Number density of coccospheres as a function of growth. (d–f) Average sizes of coccolithophores before (blue) and after complete acid dissolution (red) in the opto-electrochemical experiments. (g–i) Mean $CaCO_3$ mass per cell (left – *y* axis) and PIC : POC ratio (right – *y* axis). The error bar reports the standard error of mean and *n* is the sample size (d–i).

the new culture environment.[39] Between approximately days 2–10, cellular division is fast as can be inferred from the exponential increase in the number density until it reaches a plateau at $2 \times 10^4$, $3 \times 10^5$ and $1 \times 10^6$ cell per mL for *C. braarudii*, *G. oceanica* and *E. huxleyi*, respectively. Note that the culturing flask has a filter cap allowing air exchange but the total amount of nutrients is limited to what is initially present as detailed in ESI Section 1.† The plateau regime in the growth curve with no net increase in cell count is commonly known as the stationary phase[39] and arises from either depletion of nutrients essential for cellular division, build-up of toxins or bacterial infection.[40] Interestingly, it has been suggested that the invariance in the coccolithophore number density as seen across all three species in the stationary phase is not due to a balanced rate of 'birth and death', but arises because the cellular division rate slows to a halt.[41] Despite the near net-zero cellular division, the coccolithophores continue to grow in size.[41] The three above-mentioned growth phases, lag, exponential and stationary, are shown in Fig. 4. The green/red regime represents the transition from late-exponential into the early-stationary phase.

*In situ* optical measurements of the coccolithophores as the calcareous shell is being dissolved away by electrogenerated acid reveal, first, the size of the coccosphere *and*, at the end of the dissolution, the underlying biological cell. Fig. 4d and e shows the *average* coccolithophore radius optically measured before and after complete acid dissolution. A size decrease of both the coccosphere and the 'naked' cell are seen for *G. oceanica* and *E. huxleyi* during the exponential growth phase whilst a slight upward trend is seen for *C. braarudii*. As the rate of cellular division increases in the exponential phase, the growth time for the coccolithophores in between divisions are shortened. Consequently, this results in a decrease in cellular and coccosphere size for *G. oceanica* and *E. huxleyi* as each cellular division halves the biomass and coccoliths for individual plankton.[42] This trend is, however, not seen for *C. braarudii* possibly due to a much slower cellular division rate as compared to *G. oceanica* and *E. huxleyi*. For all three species, in the stationary phase, an increase in both the coccosphere and cellular size are seen as cellular division slows to a halt, with excellent agreement with literature observations.[40,43] Having

discussed the physiological data directly extractable from the shape transient of the coccolithophore shown in Fig. 2d, next we discuss how the PIC content can be calculated for each individual coccolithophores.

At the start of the opto-electrochemical experiment, the onset of the electrochemical potential is jumped to drive the complete oxidation of hydroquinone to form two stoichiometric equivalents of protons at the electrode interface (eqn (2)). As shown schematically in Fig. 2a, the acid diffuses from the electrode to react with the calcareous shell of the coccolithophore, which in the following is treated as a calcite-organism "core–shell" particle with the shell being $CaCO_3$. The total flux of proton, $j_{tot}$ (mol $s^{-1}$) reacting with the coccosphere is controlled by (1) how fast the protons can diffuse to the particle, *i.e.* mass transport of protons, $j_{MT}$ (mol $s^{-1}$) to a sphere on a plate,[44] and (2), the rate of heterogeneous reaction of calcite with protons, $j_{surf}$ (mol $s^{-1}$)

$$j_{tot} = \left(\frac{1}{j_{MT}} + \frac{1}{j_{surf}}\right)^{-1} \quad (3)$$

where:

$$j_{MT} = 8\pi \ln(2)(D_{H_2BQ}D_{H^+})^{0.5} c_{H_2BQ,bulk}(r_{sphere}(t))$$

and

$$j_{surf} = 8\pi R_f (r_{sphere}(t))^2 k_0 c_{H_2BQ,bulk}(D_{H_2BQ}/D_{H^+})^{0.5}$$

where $D$ is the diffusion coefficient (mol $m^{-2}$), $c_{H_2BQ,bulk}$ is the bulk concentration of the acid precursor hydroquinone ($H_2BQ$), $r_{sphere}$ is the radius of the calcite particle and is a function of time ($t$), $k_0$ is the heterogeneous rate constant (0.043 cm $s^{-1}$)[45,46] for acid dissolution of calcite in strong acid (pH < 3) and $R_f$ is the surface roughness of the calcite particle. See ESI Section 4† for further discussion on the acid dissolution kinetics of calcite and derivation of eqn (3). As can be inferred from eqn (3), in the limit of a tiny calcite particle, the overall rate of reaction is limited by the rate of surface reaction ($j_{MT} \gg j_{surf}$). On the other hand, if the calcite particle is large, the overall rate of calcite dissolution is limited by how fast the protons can diffuse to the particle interface ($j_{MT} \ll j_{surf}$). This switch-over in the acid dissolution of calcite occurs around a particle radius of 10 μm.[22,47] It is important to note that the mass-transport limited rate is proportional to the geometric size of the particle and the surface-limited rate of reaction is proportional to the specific surface area of the particle ($4\pi R_f r^2$). For the size range of coccolithophores in this study, the rate of the acid dissolution is neither limited by the mass-transport protons nor it is surface-limited, but is subject to mixed kinetics.

The total number of moles of electrogenerated acid reacting with the calcareous shell per unit time during the experiment, $j_{tot}(t)$, can be calculated knowing $r_{sphere}(t)$, which is extracted from the experiment and shown in Fig. 2d. Thus, by knowing each $CaCO_3$ reacts with 2 stoichiometric equivalents of protons, the total mass of calcite, or PIC per coccolithophore cell, can be calculated

$$PIC = \frac{RMM_{CaCO_3}}{2} \int_0^{t_{dissolved}} j_{tot}(t)\,dt \quad (4)$$

where $RMM_{CaCO_3}$ is the molar mass of $CaCO_3$ (100.1 g $mol^{-1}$) and $t_{dissolved}$ is the time at which the size of the coccosphere becomes invariant in the presence of electrogenerated acid corresponding to the total time taken for the shell to dissolve.

The $CaCO_3$ contents (PIC) calculated for *C. braarudii*, *G. oceanica* and *E. huxleyi* are shown in Fig. 4g–i and 5 using an estimated surface roughness factor ($R_f$) of 4. See ESI Section 5† for a discussion of $R_f$ and the extent of uncertainty this, among other factors, contribute towards the calculation of the $CaCO_3$ mass. Fig. 4g–i plots the *average* $CaCO_3$ mass plotted against days of growth for the three coccolithophore species and Fig. 5 shows *individual* coccolithophore $CaCO_3$ mass *versus* the volume of the calcareous shell calculated measured before and after complete acid dissolution. Unsurprisingly, *C. braarudii*, the largest out of the three species, carries the most calcium carbonate (averaging 3.0–4.5 ng $cell^{-1}$ at different parts of the growth curve), followed by *G. oceanica* (50–160 pg per cell) and *E. huxleyi* (15–35 pg per cell). These results are in good agreement with the $CaCO_3$ masses estimated by multiplying the literature reported coccolith mass range[25,30] by the expected number of ~10–20 coccoliths per cell. The estimated $CaCO_3$ per cell from literature reported coccolith values are shown in Fig. 5. For *G. oceanica* (Fig. 4h) and *E. huxleyi* (Fig. 4i), an increase in their average PIC content is clearly evidenced throughout their exponential growth followed by a drop in the PIC content as it transits into the stationary phase. In the stationary phase, an increase in PIC is seen for *E. huxleyi* but not for *G. oceanica*, no clear trend was seen for *C. braarudii*.

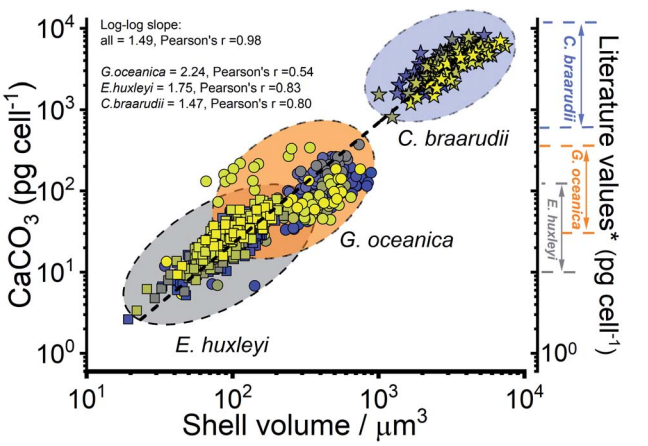


Fig. 5 Calculated calcium carbonate content of individual coccospheres plotted against the shell volume of the coccolithophore, calculated using the size before and after complete acid dissolution. Note the log–log scale. Squares – *E. huxleyi*, circles – *G. oceanica* and stars – *C. braarudii*. *The range of literature values for $CaCO_3$ mass per coccolithophore cell (pg per cell) were calculated by using the range of reported coccolith masses[25,30] multiplied by an estimate of 10–20 coccoliths per cell. The colours of the symbols represent days of growth, from day 1 (blue) to day 17 (yellow), see the legends shown in Fig. 3.

The organic carbon content of the phytoplankton cell is reported to be correlated positively with the volume of the phytoplankton cell[48]

$$\mathrm{POC} = 0.109V^{0.991} \quad (5)$$

where POC is the carbon mass (pg per cell) of the organic matter and $V$ is the volume of the phytoplankton cell ($\mu m^3$) calculated from the optically measured cellular radius after complete acid dissolution. Eqn (5) is an empirical expression derived from 30 small phytoplankton ranging from 2–60 μm, with $r^2 = 0.937$ reported in the logarithmic form.[48] The right-hand side axis of Fig. 4g–i, in blue, shows the estimated PIC : POC ratio for the three species. To compare like for like, the value of PIC used to calculate PIC : POC ratio is converted to the inorganic carbon mass (PIC = $CaCO_3$ mass cell$^{-1}$ × 12.0/100.1). *C. braarudii* has the highest PIC : POC ratio (2.0–3.0) followed by *G. oceanica* (0.2–1.0) and *E. huxleyi* (0.1–0.4). Interestingly, the PIC : POC ratio shows a similar trend to the calculated PIC as a function of phytoplankton growth.

Hitherto, physiological data of single-entity coccolithophores such as the coccosphere size, the internal cellular size, the quantity of PIC and POC are reported. It is clear that, between species, an increase in $CaCO_3$ mass is seen for the bigger coccolithophores. But a question arises, as within a species, does the amount of biomineralized $CaCO_3$ intraspecies scale with the size of the coccosphere? If so, knowing the speciation of the coccolithophore, could one then estimate the $CaCO_3$ mass empirically using *only* the size information of the coccosphere analogues to POC as shown in eqn (5). For *G. oceanica* and *E. huxleyi* it is clear from Fig. 4 that the changes in the $CaCO_3$ content along the growth curve (h and i) are not correlated with the coccosphere size (e and f). Specifically, during days 2–7 in the exponential growth an increase of $CaCO_3$ cellular content are seen for *G. oceanica* and *E. huxleyi* but their respective coccosphere and naked cell size decreases. Moreover, as *G. oceanica* transits into the stationary phase (days 8–17) an increase in the average coccosphere size is seen but the $CaCO_3$ content per cell drops. A closer look at Fig. 4d–f reveals that the size variation of the underlying 'naked' cell mirrors closely to that of the coccosphere prior to acid dissolution (cell + calcareous shell). In Fig. 5, a clear trend between the $CaCO_3$ mass and the shell volume can be seen. The latter is calculated using the optically measured radius before and after complete acid dissolution assuming a spherical shell. Since the calcareous shell is composed of inter-locking coccoliths encrusting the underlying biological cell, it is perhaps unsurprising that the $CaCO_3$ mass is not correlated to the initial coccosphere size (shell + cell), but to the volume of the calcareous shell.

## Conclusion

Single-entity measurements of calcifying coccolithophores were realised *via in situ* opto-electrochemical acid-induced dissolutions. Simultaneous optical measurement of the coccolithophore before and after complete acid dissolution reveals the calcareous shell thickness *and* the size of the underlying 'naked' cell of the same coccolithophore. This allows the following single-entity measurements to be made: PIC calculated *via* calcite dissolution kinetics, POC estimated from the volume of the 'naked' cell and, hence, an estimation of the PIC : POC ratio on a single-cell basis. We have noted the masses of biomineralized $CaCO_3$ content of individual coccolithophores varies over 3-orders of magnitudes ranging from a few picograms (*E. huxleyi*) to tens of nanograms (*C. braarudii*). These weights are too small to be measured *via* traditional methods of 'weighing'. Importantly, our data reveal that the calcification degree of the coccolithophore is *not* correlated with the size of the coccosphere but to the volume of the calcareous shell because the underlying biological cell scales proportionally with the coccosphere size. Therefore, it is impossible to resolve the calcification degree without this internal measurement.

## Author contributions

Conceptualization: MY, CBM, RGC, REMR, HAB.
Methodology: MY, CBM.
Experiment: MY (lead), SB (culture).
Formal analysis: MY.
Visualization: MY, CBM.
Supervision: RGC.
Writing—original draft: MY, CBM, RGC.
Writing—review & editing: MY, CBM, SB, RGC, REMR, HAB.

## Conflicts of interest

There are no conflicts to declare.

## Acknowledgements

This work was carried out with the support of the Oxford Martin School Programme on Monitoring Ocean Ecosystems.

## Notes and references

1 S. V. Sokolov, S. Eloul, E. Kätelhön, C. Batchelor-McAuley and R. G. Compton, *Phys. Chem. Chem. Phys.*, 2017, **19**, 28–43.
2 Y.-G. Zhou, N. V. Rees, J. Pillay, R. Tshikhudo, S. Vilakazi and R. G. Compton, *Chem. Commun.*, 2011, **48**, 224–226.
3 W. Yu, C. Batchelor-McAuley, X. Chang, N. P. Young and R. G. Compton, *Phys. Chem. Chem. Phys.*, 2019, **21**, 20415–20421.
4 R.-C. Xie, M. Volokhova, A. Boldin, L. Seinberg, M. Tsujimoto, M. Yang, B. Rasche and R. G. Compton, *ChemElectroChem*, 2020, **7**, 1261–1276.
5 L. Sepunaru, S. V. Sokolov, J. Holter, N. P. Young and R. G. Compton, *Angew. Chem., Int. Ed.*, 2016, **55**, 9768–9771.
6 S. Kuss, E. Tanner, M. Ordovas-Montanes and R. G. Compton, *Chem. Sci.*, 2017, **8**, 7682–7688.
7 L. Sepunaru, K. Tschulik, C. Batchelor-McAuley, R. Gavish and R. G. Compton, *Biomater. Sci.*, 2015, **3**, 816–820.
8 L. Sepunaru, B. J. Plowman, S. V. Sokolov, N. P. Young and R. G. Compton, *Chem. Sci.*, 2016, **7**, 3892–3899.

9 U. Passow and C. A. Carlson, *Mar. Ecol.: Prog. Ser.*, 2012, **470**, 249–271.
10 J. D. Milliman, *Global Biogeochem. Cycles*, 1993, **7**, 927–957.
11 K. M. Krumhardt, N. S. Lovenduski, M. C. Long, M. Levy, K. Lindsay, J. K. Moore and C. Nissen, *J. Adv. Model. Earth Syst.*, 2019, **11**, 1418–1437.
12 A. R. Taylor, M. A. Russell, G. M. Harper, T. f. T. Collins and C. Brownlee, *Eur. J. Phycol.*, 2007, **42**, 125–136.
13 R. A. Armstrong, C. Lee, J. I. Hedges, S. Honjo and S. G. Wakeham, *Deep Sea Res., Part II*, 2001, **49**, 219–236.
14 C. Klaas and D. E. Archer, *Global Biogeochem. Cycles*, 2002, **16**, 63.
15 T. Volk and M. I. Hoffert, *The Carbon Cycle and Atmospheric CO2: Natural Variations Archean to Present*, 1985, vol. 32, pp. 99–110.
16 M. Hain, D. Sigman and G. Haug, *Treatise Geochem.*, 2014, **8**, 485–517.
17 P. Friedlingstein, M. W. Jones, M. O'Sullivan, R. M. Andrew, D. C. Bakker, J. Hauck, C. Le Quéré, G. P. Peters, W. Peters and J. Pongratz, *Earth Syst. Sci. Data Discuss.*, 2021, 1–191.
18 B. D'Amario, C. Pérez, M. Grelaud, P. Pitta, E. Krasakopoulou and P. Ziveri, *Sci. Rep.*, 2020, **10**, 1–14.
19 A. Ridgwell, D. Schmidt, C. Turley, C. Brownlee, M. Maldonado, P. Tortell and J. Young, *Biogeosciences*, 2009, **6**, 2611–2623.
20 J. J. Kharbush, H. G. Close, B. A. Van Mooy, C. Arnosti, R. H. Smittenberg, F. A. Le Moigne, G. Mollenhauer, B. Scholz-Böttcher, I. Obreht and B. P. Koch, *Front. Mar. Sci.*, 2020, **7**, 518.
21 P. R. Bown, J. A. Lees and J. R. Young, in *Coccolithophores*, Springer, 2004, pp. 481–508.
22 M. Yang, C. Batchelor-McAuley, S. Barton, R. E. M. Rickaby, H. A. Bouman and R. G. Compton, *Angew. Chem.*, 2021, **133**, 21167–21174.
23 M.-Á. Fuertes, J.-A. Flores and F. J. Sierro, *Mar. Micropaleontol.*, 2014, **113**, 44–55.
24 L. Beaufort, N. Barbarin and Y. Gally, *Nat. Protoc.*, 2014, **9**, 633–642.
25 J. R. Young and P. Ziveri, *Deep Sea Res., Part II*, 2000, **47**, 1679–1700.
26 G. Langer, M. Geisen, K.-H. Baumann, J. Kläs, U. Riebesell, S. Thoms and J. R. Young, *Geochem., Geophys., Geosyst.*, 2006, **7**, Q09006.
27 P. G. Matson, T. M. Ladd, E. R. Halewood, R. P. Sangodkar, B. F. Chmelka and M. D. Iglesias-Rodriguez, *PLoS One*, 2016, **11**, e0162313.
28 X. Jin, C. Liu, A. J. Poulton, M. Dai and X. Guo, *Biogeosciences*, 2016, **13**, 4843–4861.
29 S. A. O'Dea, S. J. Gibbs, P. R. Bown, J. R. Young, A. J. Poulton, C. Newsam and P. A. Wilson, *Nat. Commun.*, 2014, **5**, 1–7.
30 T. Beuvier, I. Probert, L. Beaufort, B. Suchéras-Marx, Y. Chushkin, F. Zontone and A. Gibaud, *Nat. Commun.*, 2019, **10**, 1–8.
31 R. Hoffmann, C. Kirchlechner, G. Langer, A. S. Wochnik, E. Griesshaber, W. W. Schmahl and C. Scheu, *Biogeosciences*, 2015, **12**, 825–834.
32 M. Yang, C. Batchelor-McAuley, L. Chen, Y. Guo, Q. Zhang, R. E. M. Rickaby, H. A. Bouman and R. G. Compton, *Chem. Sci.*, 2019, **10**, 7988–7993.
33 M. Andersson, C. Hem, L. Schultz, J. Nielsen, C. Pedersen, K. Sand, D. Okhrimenko, A. Johnsson and S. Stipp, *J. Phys. Chem. A*, 2014, **118**, 10720–10729.
34 J. W. Anthony, *Handbook of Mineralogy: Borates, Carbonates, Sulfates*, Mineral Data Pub, 1990.
35 K. Lund, H. S. Fogler, C. McCune and J. Ault, *Chem. Eng. Sci.*, 1975, **30**, 825–835.
36 C. E. Walker, S. Heath, D. L. Salmon, N. Smirnoff, G. Langer, A. R. Taylor, C. Brownlee and G. L. Wheeler, *Front. Mar. Sci.*, 2018, **5**, 306.
37 T. J. Davies, C. E. Banks and R. G. Compton, *J. Solid State Electrochem.*, 2005, **9**, 797–808.
38 R. G. Compton and C. E. Banks, *Understanding Voltammetry*, World Scientific, Singapore, 2018.
39 G. E. Fogg and B. Thake, *Algal Cultures and Phytoplankton Ecology*, Univ of Wisconsin Press, 1987.
40 I. Zondervan, *Deep Sea Res., Part II*, 2007, **54**, 521–537.
41 S. J. Gibbs, A. J. Poulton, P. R. Bown, C. J. Daniels, J. Hopkins, J. R. Young, H. L. Jones, G. J. Thiemann, S. A. O'Dea and C. Newsam, *Nat. Geosci.*, 2013, **6**, 218–222.
42 C. E. Walker, A. R. Taylor, G. Langer, G. M. Durak, S. Heath, I. Probert, T. Tyrrell, C. Brownlee and G. L. Wheeler, *New Phytol.*, 2018, **220**, 147–162.
43 E. Paasche, *Eur. J. Phycol.*, 1998, **33**, 33–42.
44 P. Bobbert, M. Wind and J. Vlieger, *Phys. A*, 1987, **141**, 58–72.
45 R. G. Compton and P. R. Unwin, *Philos. Trans. R. Soc., A*, 1990, **330**, 1–45.
46 R. G. Compton, K. L. Pritchard and P. R. Unwin, *J. Chem. Soc., Chem. Commun.*, 1989, 249–251.
47 R. G. Comptom, K. L. Pritchard and P. R. Unwin, *Freshwater Biol.*, 1989, **22**, 285–288.
48 D. J. Montagnes, J. A. Berges, P. J. Harrison and F. Taylor, *Limnol. Oceanogr.*, 1994, **39**, 1044–1060.